

Rapid generation and number-resolved detection of spinor rubidium Bose-Einstein condensatesCebrail Pür,^{1,*} Mareike Hetzel^{1,*},[†] Martin Quensen¹, Andreas Hüper^{1,2}, Jiao Geng,^{3,4} Jens Kruse,^{1,2} Wolfgang Ertmer,^{1,2} and Carsten Klempt^{1,2}¹*Institut für Quantenoptik, Leibniz Universität Hannover, Welfengarten 1, D-30167 Hannover, Germany*²*Deutsches Zentrum für Luft- und Raumfahrt e.V. (DLR), Institut für Satellitengeodäsie und Inertialsensorik (DLR-SI), Callinstraße 30b, D-30167 Hannover, Germany*³*Key Laboratory of 3D Micro/Nano Fabrication and Characterization of Zhejiang Province, School of Engineering, Westlake University, 18 Shilongshan Road, Hangzhou 310024, Zhejiang Province, China*⁴*Institute of Advanced Technology, Westlake Institute for Advanced Study, 18 Shilongshan Road, Hangzhou 310024, Zhejiang Province, China*

(Received 1 July 2022; revised 17 January 2023; accepted 20 January 2023; published 6 March 2023)

High data acquisition rates and low-noise detection of ultracold neutral atoms present important challenges for the state tomography and interferometric application of entangled quantum states in Bose-Einstein condensates. In this paper, we present a high-flux source of ⁸⁷Rb Bose-Einstein condensates combined with a number-resolving detection. We create Bose-Einstein condensates of 2×10^5 atoms with no discernible thermal fraction within 3.3 s using a hybrid evaporation approach in a magnetic and optical trap. For the high-fidelity tomography of many-body quantum states in the spin degree of freedom [M. Hetzel, *et al.*, [arXiv:2207.01270](https://arxiv.org/abs/2207.01270)], it is desirable to select a single mode for a number-resolving detection. We demonstrate the low-noise selection of subsamples of up to 16 atoms and their subsequent detection with a counting noise below 0.2 atoms. The presented techniques offer an exciting path towards the creation and analysis of mesoscopic quantum states with improved fidelities and towards their exploitation for fundamental and metrological applications.

DOI: [10.1103/PhysRevA.107.033303](https://doi.org/10.1103/PhysRevA.107.033303)**I. HIGH-FLUX SOURCES OF BOSE-EINSTEIN CONDENSATES**

Because of their well-controlled spatial mode and their phase coherence, Bose-Einstein condensates (BECs) of neutral atoms present a valuable resource for atom interferometry and quantum atom optics experiments in general. Many of the applications, however, require short preparation times. In atom interferometry, the preparation time defines the dead time of the sensor and therefore influences bandwidth and noise sensitivity. Short preparation times are also important as they often dominate the data acquisition rate. In our case, we wish to generate entangled many-body states and perform a high-fidelity state tomography. The number of required measurements scales exponentially with the number of atoms. Therefore an accurate characterization of quantum states with an increasing number of atoms requires the acquisition of large data sets, during which the environmental conditions have to remain stable. An improvement of the measurement rate not only improves the quality of the results, but also in fact constitutes a requirement for scaling up the number of atoms in the generation of high-fidelity quantum states.

Besides a few exceptions [1,2], BECs are typically realized by forced evaporative cooling in conservative potentials

resulting from inhomogeneous magnetic or optical fields. Figure 1 displays a selection of atom numbers and repetition rates obtained with atom-chip magnetic traps [3–7], macroscopic magnetic traps [8–14], all-optical traps [15–22], and combinations of magnetic and optical traps [23–26].

For our experiments, we aim at BECs with 10^5 rubidium atoms at a maximal repetition rate. At the same time, the setup is supposed to enable the selection and detection of subensembles with single-particle counting resolution. The inclusion of such a high-performance detection excludes the implementation of an atom chip, which would promise short preparation times but leads to detrimental light scattering on the chip surface.

In this paper, we present our experimental setup, which enables the generation of 2×10^5 rubidium atoms with a cycle time of 3.3 s and the number-resolving detection of a subensemble in a specific spin state. The BEC generation relies on a macroscopic quadrupole trap combined with a crossed-beam optical dipole trap (cODT). The fluorescence detection is a fiber-based second generation from an earlier implementation [27]. This paper describes the experimental setup and the obtained results, also as a reference for the quantum detector tomography reported in Ref. [28].

This paper is organized as follows. In Sec. II, we describe the details of our apparatus and our experimental sequence for fast BEC production. Section III presents the successive spin preparation of small ensembles by microwave transitions and subsequent optical removal of atoms. The number-resolving detection setup is described in Sec. IV. Section V concludes with a summary and outlook.

*These authors contributed equally to this work.

[†]Author to whom correspondence should be addressed: hetzel@iqo.uni-hannover.de

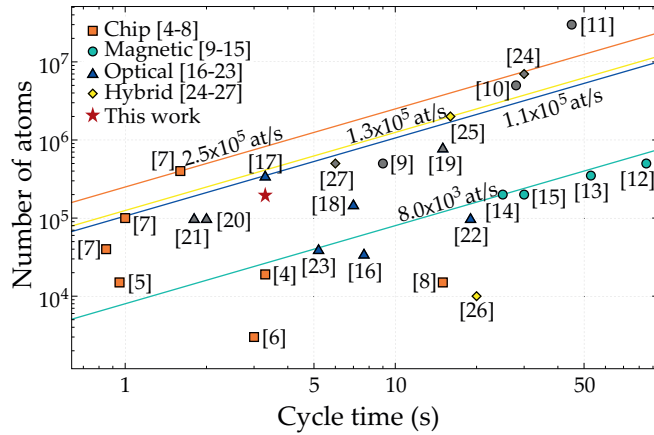


FIG. 1. Overview of the production time for different BEC sources with a given final atom number. Orange squares are atom-chip-based experiments, teal circles correspond to magnetically trapped ensembles, blue triangles show all-optical evaporation, and yellow diamonds represent hybrid magnetic and optical methods. Sources featuring other atomic species than rubidium are marked in gray. The red star marks the result of this work corresponding to an atomic flux of 6×10^4 atoms/s. Solid lines illustrate the atomic flux of the best-performing experiments per category.

II. RAPID CREATION OF BOSE-EINSTEIN CONDENSATES

The experimental setup (Fig. 2) consists of two glass cells which are connected by two sequential differential pumping stages. The first, rectangular cell ($150 \times 60 \times 60$ mm) contains a two-dimensional magneto-optical trap ($2D^+$ MOT). The second, octagonal glass cell (seven 1-in. and two 3-in.

viewports) contains a 3D MOT, and further experiments are carried out. The experimental sequence is initiated by loading the MOT and continues with the BEC creation and the mode-selective detection (Fig. 3). The design of the $2D^+$ MOT is described in Ref. [29]. The 3D MOT is operated with a coil pair of 20 windings each in the vertical direction, yielding 12 G/cm at 103 A. The cooling and detection laser light is generated by two external-cavity diode lasers [30], frequency stabilized via modulation transfer spectroscopy [31], and four tapered amplifiers. Optical fibers deliver the light to the vacuum setup, where the light power is actively stabilized. Here six beams with a power of 35 mW and a waist of 7.5 mm are formed and enter the glass cell via the 3-in. windows at an angle of 45° . This beam configuration offers large optical access for detection with a numerical aperture $NA = 0.42$. The glass cell is antireflection-coated on both sides for 780-nm light to maximally suppress background light during the fluorescence detection. The initial loading rate of our 3D MOT is 2.4×10^{10} atoms/s, and within 200 ms, 4×10^9 atoms are captured.

After MOT loading, an optical molasses cools the atoms to 18 μ K. The atoms are optically pumped to the level $|F, m_F\rangle = |2, 2\rangle$ on the $D2 F = 2 \rightarrow F' = 2$ transition and loaded into a magnetic quadrupole trap (QPT). The magnetic field gradient, generated by a coil pair with 62 windings each, is linearly ramped up from 58 to 169 G/cm in 50 ms. The currents are measured by current transducers and actively stabilized to better than 10^{-4} relative stability. The $1/e$ lifetime cannot be measured during the maximally allowed continuous operation of 10 s and exceeds 150 s. We perform evaporation by two linear radio-frequency (rf) ramps from 20 to 3.5 MHz within 1.6 s.

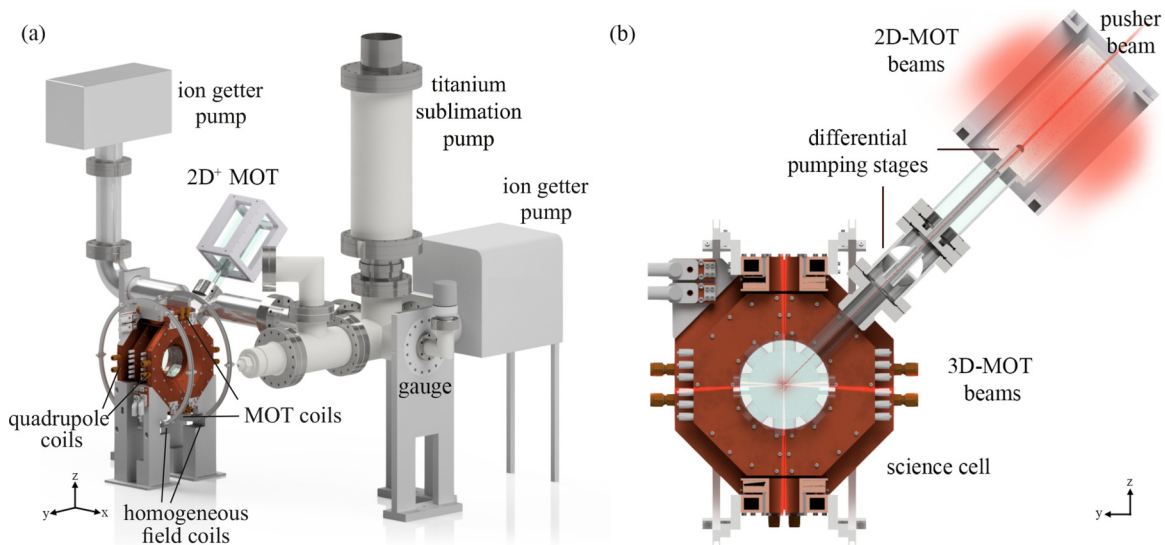


FIG. 2. (a) Computer-aided design of the ultrahigh-vacuum system with the two-chamber setup and the coil system. The system contains two glass cells for the $2D^+$ MOT and for the 3D MOT and BEC generation, which are connected via two differential pumping stages at a 45° angle. The connection tube and the science cell are individually pumped by two pump arrangements. The coil system surrounding the science cell is assembled by a pair of vertical 3D-MOT coils, a pair of horizontal quadrupole coils, and a pair of orthogonally aligned Helmholtz coils. The science cell and the coil arrangement are optimized for a high-NA optical access along the x direction. (b) Cross section of the two-chamber setup and the coil system. Atoms are released from dispensers, building up the pressure inside the $2D^+$ MOT. A pusher beam guides the $2D^+$ -MOT beam through the two differential pumping stages into the science chamber, where they are captured and cooled.

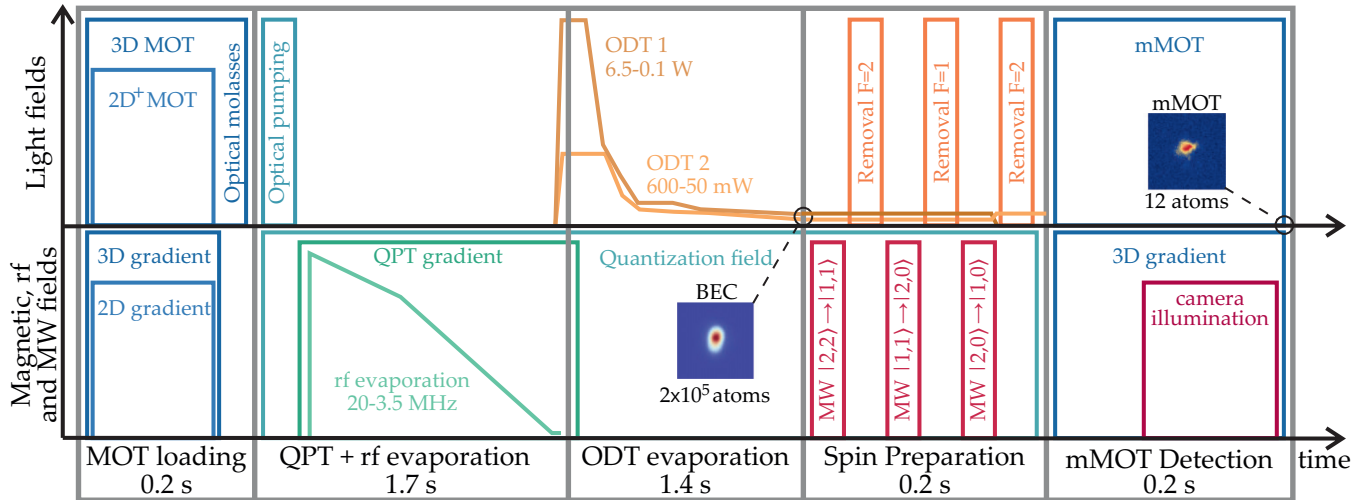


FIG. 3. Schematic of the experimental sequence. The upper and lower panels illustrate the light and magnetic fields, respectively. The field strengths and the time axis are not to scale. The BEC is created within 3.3 s in a hybrid evaporation approach in a magnetic and optical trap. Subsequently, the desired spin component is chosen and analyzed in the number-resolving mMOT setup.

Afterwards, a crossed-beam optical dipole trapping potential is added with a trap center slightly below the magnetic trap center [24,32]. The optical dipole potential is generated by a 55-W Coherent Mephisto master oscillator power amplifier (MOPA) laser with a wavelength of 1064 nm. Two beams, whose intensities are each stabilized via an acousto-optic deflector (AOD), enter the glass cell via free-space optics along the x and y directions with waists of 70 and 35 μm , respectively. The power is increased to 6.5 W and 600 mW within 200 ms, and the quadrupole field is ramped to zero within another 200 ms. Finally, the power of the dipole trap beams is decreased in six linear ramps to final values of 95 and 45 mW within 1.2 s resulting in simulated trap frequencies of $(\omega_x, \omega_y, \omega_z) = 2\pi \times (60, 160, 150)$ Hz.

The evaporation is optimized for speed instead of atom number yielding an evaporation efficiency of $\gamma = 1.7$. After the final evaporation, we obtain BECs of 2×10^5 atoms with no discernible thermal fraction. The total BEC preparation takes 3.3 s. Due to an insufficient cooling of the quadrupole trap coils, this cycle rate can so far only be maintained for 200 repetitions. An operation for longer times requires an additional 2 s cooldown time or an improvement in the water cooling which is planned for the future.

III. SELECTION OF A SUBENSEMBLE IN A SPECIFIC SPIN STATE

After the rapid creation of a BEC, we aim at the generation of many-body spin states and their analysis by selecting one spin mode for number-resolved detection. This spin-selective number detection is the prerequisite of the characterization of a coherent spin state in Ref. [28]. Here, we demonstrate that a particular spin component can be chosen for detection with a fluorescence-based number counting. The technique is demonstrated for up to 16 atoms but can be extended to several hundred atoms in the near future. While this number seems to be small at first glance, we would like to highlight that this spin-selective detection allows for a tomography of

multiparticle states with much larger atom numbers, as long as they are sufficiently polarized (e.g., spin-squeezed states). As an example, we transfer a variable number of atoms to the spin level $|1, 0\rangle$ while we remove all remaining components in the $F = 2$ manifold. The atoms in level $|1, 0\rangle$ are counted in a fiber-based miniature magneto-optical trap (mMOT). The same technique can be implemented for a large variety of many-particle spin states to select a specific spin level for counting. For the creation of many of these states, an ensemble in the spin level $|1, 0\rangle$ serves as a starting point. Therefore we characterize the necessary techniques by preparing and detecting a small fraction of the BEC in $|1, 0\rangle$. We select a subensemble of the BEC that we transfer into the spin level $|1, 1\rangle$ by choosing the length of the microwave (MW) pulse as a fraction of its π -pulse length. We remove the remaining components in the $F = 2$ manifold by a 100- μs resonant cooling light push. In the following, a MW π pulse transfers the atoms to the spin level $|2, 0\rangle$. To ensure there are no remaining fractions in $F = 1$ caused by a nonperfect MW transfer, we employ a 100- μs resonant repumping light push. A final MW pulse transfers the atoms into the spin level $|1, 0\rangle$, and another removal of atoms in $F = 2$ ensures the detection of the desired components in $F = 1$. Between the optical removals, short waiting times on the order of 10 ms have been implemented to guarantee that the mechanical shutters open and close reliably. The transfer of atoms to the level $|1, 0\rangle$ from the initially prepared level $|2, 2\rangle$ is carried out by a low-noise microwave source [33]. The quantization axis is given by a magnetic field of 0.78 G, which is actively stabilized to a magnetic field sensor, yielding a magnetic field noise of 170 μG .

A counting resolution on the single-atom level places strong requirements on the efficiency and selectivity of the final removal process. Two effects deteriorate the counting precision: (i) Atoms expelled from the trap may collide with atoms that are selected for detection and remove them unintentionally. (ii) The resonant light that is used to expel the $F = 2$ atoms may pump atoms into the nonresonant $F = 1$ levels before they leave the trap. To avoid unwanted loss

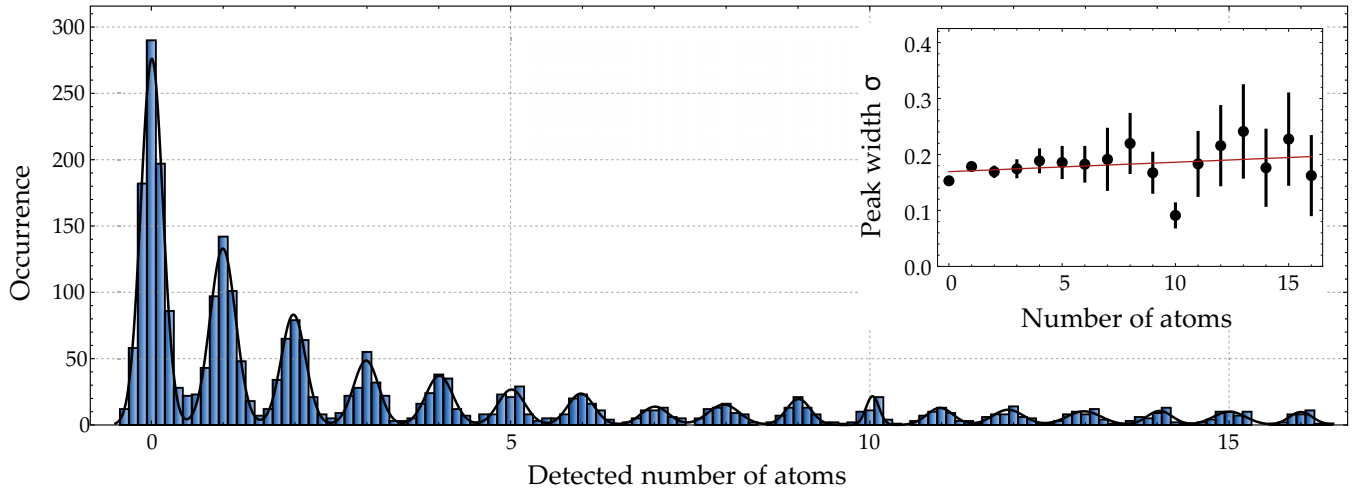


FIG. 4. Histogram of the fluorescence signal for up to 16 atoms. The signal (blue bars) shows a clear quantization for integer atom numbers. The individual peaks are fitted with Gaussian distributions (black curve), whose widths are shown in the inset. The linear fit (solid red line in the inset) is compatible with a previously determined single-particle resolution limit of 400 atoms.

due to collisions during the optical removal, we transfer the atoms into a single-beam optical dipole trap. Pumping the atoms into a closed cycling transition reduces the probability of populating nonresonant states. Therefore we use a homogeneous magnetic field of 6.7 G and a σ^+ -polarized light beam for optical removal of the $F = 2$ manifold before we detect the atoms in $F = 1$ in our number-resolving mMOT setup. To avoid recapturing the previously removed atoms, we implement a waiting time of 150 ms after the final removal before detection.

IV. NUMBER-RESOLVING DETECTION

We detect the number of selected atoms in the $F = 1$ manifold with an improved mMOT setup that is based on the system described in Ref. [27]. The initial version of the detection setup included beams distributed via free-space optics so that they could be superimposed with the larger MOT beams creating our 3D MOT for BEC generation. This setup proved to be capable of accurate atom counting, but it showed long-term instabilities due to the long beam paths. The updated version therefore features six fiber-based beams minimizing the optical path lengths. Each fiber is individually mounted, and its output intensity is actively stabilized, enabling a precise balancing of the intensities of the counter-propagating beams. The exact position of the mMOT depends on several parameters, including the magnetic field minimum, the precise beam alignment, and the beams' intensity balance. To precisely overlap the mMOT with the BEC position, the mMOT beams are aligned onto the BEC position. Homogeneous magnetic fields in both horizontal directions shift the magnetic field minimum to the BEC position. The beam intensities and thereby the exact mMOT position have been optimized by a differential evolution algorithm [34], because the nontrivial interference of the beams leads to jumps in the mMOT position. The mMOT is operated at a magnetic field gradient of 12 G/cm with a detuning of 10 MHz (1.7Γ) and an intensity of six times the saturation intensity. Due to spatial constraints, the new horizontal beams enter the science

glass cell at an angle of 35° . This changed angle results in a higher background scattering in our detection objective and therefore in higher background noise $\sigma_{bg,new} = 0.15$ compared with 0.03 in the previous setup [27]. Figure 4 shows a histogram of the recorded fluorescence signal for 2433 repeated number measurements of atoms in the level $|1, 0\rangle$. The histogram shows a clear quantization of the fluorescence signal, proving a counting resolution well below the single-atom limit. The counting noise depends on the total number of atoms and is well described by Gaussian functions with a width $\sigma_N = 0.169 + 0.0017N$. Assuming a linear scaling, this allows for single-particle detection of more than 400 atoms, in correspondence to our earlier quantification [27]. The data can now be binned at half-integer binning limits, with a number assignment fidelity ranging from 99.7% at 1 atom to 99.0% at 15 atoms.

The mMOT has a finite probability of capturing unwanted atoms from the background gas. These atoms are mainly captured because of the frequent use of the $2D^+$ MOT during the BEC creation, leading to a temporally increased background pressure. Atoms passing the small but still relevant trapping volume of the mMOT can be trapped and therefore counted in the detection process. This results in a detection offset of 0.27 atoms, which appears as a relevant signal in the quantum tomography of our number detection [28].

The effects contributing to the detection offset are characterized in Fig. 5. Figure 5(a) shows the unwanted background loading of the mMOT, once in the beginning (cyan rectangles) and once after 7.5 h of continuous operation (blue circles). The increase from 0.1 to 3.4 atoms/s extracted from linear fits is caused by the temporary increase of the background gas that builds up over time. We find that this buildup is generated by laser-cooled atoms in the $2D^+$ -MOT beam and not by thermal atoms passing the two differential pumping stages.

To maintain accurate atom number counting, the loading of atoms from the background gas has to be minimized, which poses a limit to the total mMOT operation time. At the same time, our single-particle counting resolution demands long illumination times. A total mMOT operation time of

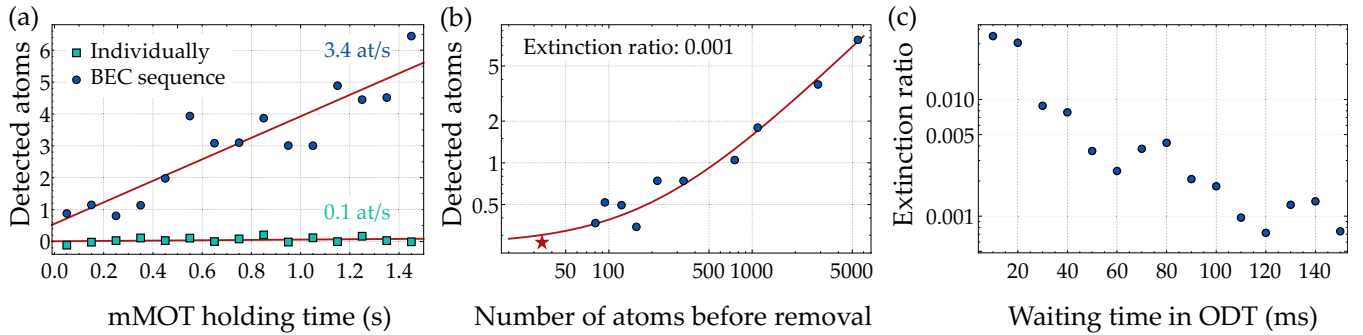


FIG. 5. Characterization of the detection offset. (a) The frequent use of the $2D^+$ MOT temporarily increases the background gas and therefore the mMOT loading rate from initially 0.1 atoms/s (cyan rectangles) to 3.4 atoms/s (blue circles) after 7.5 h of operation. (b) The detection offset linearly depends on the number of atoms before removal. The red curve shows a linear fit with an initial offset that is caused by a nonperfect optical removal of atoms. The red star marks the detection offset in Ref. [28]. (c) The extinction ratio of the optical removal improves with an increasing subsequent waiting time before detection.

115 ms including 65 ms for illumination yields a reasonable compromise. Figure 5(b) shows the linear dependence of the detection offset on the number of removed atoms N_{rem} . Nonperfect optical removals and increased recapturing of previously removed atoms both contribute to this increasing detection offset N_{off} following $N_{\text{off}} = 0.26 + 0.001N_{\text{rem}}$. The red star illustrates the detection offset obtained in Ref. [28]. Figure 5(c) illustrates the dependence of the extinction ratio on the waiting time after the optical removal. A waiting time of 150 ms reduces the probability of recapturing previously removed atoms in the mMOT by more than one order of magnitude. In summary, the described detection enables a number-resolving tomography of quantum many-body states up to a few hundred atoms.

V. CONCLUSION AND OUTLOOK

In conclusion, we have presented a method for the generation and number-resolved detection of spinor BECs. We create BECs with 2×10^5 ^{87}Rb atoms within 3.3 s using a hybrid approach. The high-flux atom source consists of a $2D^+$ MOT combined with a 3D MOT. After transfer into a magnetic quadrupole trap, a first rf-evaporation step is applied to increase the phase space density and to efficiently transfer the atoms into the optical dipole potential, in which fast efficient evaporation is performed. Our experiment shows a high-flux BEC creation of 6×10^4 atoms/s, which is close

to the published record for Rb [24], disregarding the atom-chip experiments which do not provide sufficient optical access. The cycle time can be further improved by decreasing the evaporation time in the crossed optical dipole trap. We can readily implement dynamically shaped potentials using our acousto-optical deflector setup, which will give us independent control of the trap depth and trapping frequencies, leading to accelerated evaporation dynamics.

We select a single spin level for detection and optically remove residual atoms with an extinction ratio of 0.001. We resolve the created output states with a detection offset of 0.27 atoms and a number assignment fidelity of 99% at 15 atoms. The presented techniques pave the way for the high-fidelity tomography of polarized many-particle entangled states, such as single- and two-mode spin-squeezed states.

ACKNOWLEDGMENTS

This work is supported by the QuantERA grants SQUEIS and MENTA. We acknowledge financial support from the Deutsche Forschungsgemeinschaft (DFG, German Research Foundation) - Project-ID 274200144 - SFB 1227 DQ-mat within Project No. B01 and Germany's Excellence Strategy - EXC-2123 QuantumFrontiers - Project No. 390837967. M.Q. acknowledges support from the Hannover School for Nanotechnology (HSN).

-
- [1] A. Urvoy, Z. Vendeiro, J. Ramette, A. Adiyatullin, and V. Vuletić, Direct Laser Cooling to Bose-Einstein Condensation in a Dipole Trap, *Phys. Rev. Lett.* **122**, 203202 (2019).
 - [2] S. Stellmer, B. Pasquiou, R. Grimm, and F. Schreck, Laser Cooling to Quantum Degeneracy, *Phys. Rev. Lett.* **110**, 263003 (2013).
 - [3] D. M. Farkas, K. M. Hudek, E. A. Salim, S. R. Segal, M. B. Squires, and D. Z. Anderson, A compact, transportable, microchip-based system for high repetition rate production of Bose-Einstein condensates, *Appl. Phys. Lett.* **96**, 093102 (2010).
 - [4] D. M. Farkas, E. A. Salim, and J. Ramirez-Serrano, Production of rubidium Bose-Einstein condensates at a 1 Hz rate, [arXiv:1403.4641](https://arxiv.org/abs/1403.4641).
 - [5] M. Horikoshi and K. Nakagawa, Atom chip based fast production of Bose-Einstein condensate, *Appl. Phys. B* **82**, 363 (2006).
 - [6] J. Rudolph, W. Herr, C. Grzeschik, T. Sternke, A. Grote, M. Popp, D. Becker, H. Müntinga, H. Ahlers, A. Peters, C. Lämmerzahl, K. Sengstock, N. Gaaloul, W. Ertmer, and E. M. Rasel, A high-flux BEC source for mobile atom interferometers, *New J. Phys.* **17**, 065001 (2015).

- [7] S. Abend, M. Gebbe, M. Gersemann, H. Ahlers, H. Müntinga, E. Giese, N. Gaaloul, C. Schubert, C. Lämmerzahl, W. Ertmer, W. P. Schleich, and E. M. Rasel, Atom-Chip Fountain Gravimeter, *Phys. Rev. Lett.* **117**, 203003 (2016).
- [8] K. B. Davis, M. O. Mewes, M. R. Andrews, N. J. van Druten, D. S. Durfee, D. M. Kurn, and W. Ketterle, Bose-Einstein Condensation in a Gas of Sodium Atoms, *Phys. Rev. Lett.* **75**, 3969 (1995).
- [9] M.-O. Mewes, M. R. Andrews, N. J. van Druten, D. M. Kurn, D. S. Durfee, and W. Ketterle, Bose-Einstein Condensation in a Tightly Confining dc Magnetic Trap, *Phys. Rev. Lett.* **77**, 416 (1996).
- [10] D. S. Naik and C. Raman, Optically plugged quadrupole trap for Bose-Einstein condensates, *Phys. Rev. A* **71**, 033617 (2005).
- [11] T. Esslinger, I. Bloch, and T. W. Hänsch, Bose-Einstein condensation in a quadrupole-Ioffe-configuration trap, *Phys. Rev. A* **58**, R2664(R) (1998).
- [12] S. Kumar, S. Sarkar, G. Verma, C. Vishwakarma, M. Noaman, and U. Rapol, Bose-Einstein condensation in an electro-pneumatically transformed quadrupole-Ioffe magnetic trap, *New J. Phys.* **17**, 023062 (2015).
- [13] R. Dubessy, K. Merloti, L. Longchambon, P.-E. Pottie, T. Liennard, A. Perrin, V. Lorent, and H. Perrin, Rubidium-87 Bose-Einstein condensate in an optically plugged quadrupole trap, *Phys. Rev. A* **85**, 013643 (2012).
- [14] S. Peil, J. V. Porto, B. Laburthe Tolra, J. M. Obrecht, B. E. King, M. Subbotin, S. L. Rolston, and W. D. Phillips, Patterned loading of a Bose-Einstein condensate into an optical lattice, *Phys. Rev. A* **67**, 051603(R) (2003).
- [15] M. D. Barrett, J. A. Sauer, and M. S. Chapman, All-Optical Formation of an Atomic Bose-Einstein Condensate, *Phys. Rev. Lett.* **87**, 010404 (2001).
- [16] T. Kinoshita, T. Wenger, and D. S. Weiss, All-optical Bose-Einstein condensation using a compressible crossed dipole trap, *Phys. Rev. A* **71**, 011602(R) (2005).
- [17] J.-F. Clément, J.-P. Brantut, M. Robert-de Saint-Vincent, R. A. Nyman, A. Aspect, T. Bourdel, and P. Bouyer, All-optical runaway evaporation to Bose-Einstein condensation, *Phys. Rev. A* **79**, 061406(R) (2009).
- [18] M. Landini, S. Roy, G. Roati, A. Simoni, M. Inguscio, G. Modugno, and M. Fattori, Direct evaporative cooling of ^{39}K atoms to Bose-Einstein condensation, *Phys. Rev. A* **86**, 033421 (2012).
- [19] S. Stellmer, R. Grimm, and F. Schreck, Production of quantum-degenerate strontium gases, *Phys. Rev. A* **87**, 013611 (2013).
- [20] R. Roy, A. Green, R. Bowler, and S. Gupta, Rapid cooling to quantum degeneracy in dynamically shaped atom traps, *Phys. Rev. A* **93**, 043403 (2016).
- [21] D. Xie, D. Wang, W. Gou, W. Bu, and B. Yan, Fast production of rubidium Bose-Einstein condensate in a dimple trap, *J. Opt. Soc. Am. B* **35**, 500 (2018).
- [22] G. Condon, M. Rabault, B. Barrett, L. Chichet, R. Arguel, H. Eneriz-Imaz, D. Naik, A. Bertoldi, B. Battelier, P. Bouyer, and A. Landragin, All-Optical Bose-Einstein Condensates in Microgravity, *Phys. Rev. Lett.* **123**, 240402 (2019).
- [23] G. Colzi, E. Fava, M. Barbiero, C. Mordini, G. Lamporesi, and G. Ferrari, Production of large Bose-Einstein condensates in a magnetic-shield-compatible hybrid trap, *Phys. Rev. A* **97**, 053625 (2018).
- [24] Y.-J. Lin, A. R. Perry, R. L. Compton, I. B. Spielman, and J. V. Porto, Rapid production of ^{87}Rb Bose-Einstein condensates in a combined magnetic and optical potential, *Phys. Rev. A* **79**, 063631 (2009).
- [25] M. Zaiser, J. Hartwig, D. Schlippert, U. Velte, N. Winter, V. Lebedev, W. Ertmer, and E. M. Rasel, Simple method for generating Bose-Einstein condensates in a weak hybrid trap, *Phys. Rev. A* **83**, 035601 (2011).
- [26] Q. Bouton, R. Chang, A. L. Hoendervanger, F. Nogrette, A. Aspect, C. I. Westbrook, and D. Clément, Fast production of Bose-Einstein condensates of metastable helium, *Phys. Rev. A* **91**, 061402(R) (2015).
- [27] A. Hüper, C. Pür, M. Hetzel, J. Geng, J. Peise, I. Kruse, M. Kristensen, W. Ertmer, J. Arlt, and C. Klempt, Number-resolved preparation of mesoscopic atomic ensembles, *New J. Phys.* **23**, 113046 (2021).
- [28] M. Hetzel, L. Pezzè, C. Pür, M. Quensen, A. Hüper, J. Geng, J. Kruse, L. Santos, W. Ertmer, A. Smerzi, and C. Klempt, Tomography of a number-resolving detector by reconstruction of an atomic many-body quantum state, [arXiv:2207.01270](https://arxiv.org/abs/2207.01270).
- [29] S. Jöllnbeck, J. Mahnke, R. Randoll, W. Ertmer, J. Arlt, and C. Klempt, Hexapole-compensated magneto-optical trap on a mesoscopic atom chip, *Phys. Rev. A* **83**, 043406 (2011).
- [30] X. Baillard, A. Gauguier, S. Bize, P. Lemonde, P. Laurent, A. Clairon, and P. Rosenbusch, Interference-filter-stabilized external-cavity diode lasers, *Opt. Commun.* **266**, 609 (2006).
- [31] D. J. McCarron, S. A. King, and S. L. Cornish, Modulation transfer spectroscopy in atomic rubidium, *Meas. Sci. Technol.* **19**, 105601 (2008).
- [32] G. Kleine Büning, J. Will, W. Ertmer, C. Klempt, and J. Arlt, A slow gravity compensated atom laser, *Appl. Phys. B* **100**, 117 (2010).
- [33] B. Meyer, A. Idel, F. Anders, J. Peise, and C. Klempt, Dynamical low-noise microwave source for cold atom experiments, [arXiv:2003.10989](https://arxiv.org/abs/2003.10989).
- [34] I. Geisel, K. Cordes, J. Mahnke, S. Jöllnbeck, J. Ostermann, J. Arlt, W. Ertmer, and C. Klempt, Evolutionary optimization of an experimental apparatus, *Appl. Phys. Lett.* **102**, 214105 (2013).